molecules

MDPI

Article

Keep Your TEMPO Up: Nitroxide Radicals as Sensors of Intermolecular Interactions

Ilya G. Shenderovich

Institute of Organic Chemistry, University of Regensburg, Universitaetstrasse 31, 93053 Regensburg, Germany; ilya.shenderovich@ur.de

Abstract: This study examines experimental data on the influence of the surrounding medium and non-covalent interactions on the isotropic hyperfine coupling constant, $A_{iso}(^{14}N)$, of the stable nitroxide radical 2,2,6,6-Tetramethylpiperidin-1-yl)oxyl (TEMPO) in solution. The data were used to identify a density functional theory functional/basis set combination that accurately reproduces the experimental $A_{iso}(^{14}N)$ values. The variations in $A_{iso}(^{14}N)$ due to external factors are two orders of magnitude greater than the accuracy of its experimental measurements, making $A_{iso}(^{14}N)$ a highly sensitive experimental probe for quantifying these effects. Additionally, it was found that the proton-accepting ability of the N-O$^{\bullet}$ moiety in TEMPO resembles that of the P=O moiety, enabling the simultaneous formation of two equally strong hydrogen bonds.

Keywords: TEMPO; EPR; hyperfine coupling constant; hydrogen bonding; non-covalent interactions

check for updates

Citation: Shenderovich, I.G. Keep Your TEMPO Up: Nitroxide Radicals as Sensors of Intermolecular Interactions. *Molecules* **2024**, *29*, 5032. https://doi.org/10.3390/molecules29215032

Academic Editor: Benedito José Costa Cabral

Received: 14 October 2024
Revised: 22 October 2024
Accepted: 23 October 2024
Published: 24 October 2024

Copyright: © 2024 by the author. Licensee MDPI, Basel, Switzerland. This article is an open access article distributed under the terms and conditions of the Creative Commons Attribution (CC BY) license (https://creativecommons.org/licenses/by/4.0/).

1. Introduction

The interaction of molecules with nitroxide radicals induces several characteristic spectral changes. This interaction affects the chemical shifts and relaxation times of the nuclei, as well as the appearance of the unpaired electron spin density on these nuclei. The most important actual application of stable radicals is the technique of dynamic nuclear polarization (DNP) [1]. This technique has many applications for molecular systems of varying complexity [2–6].

Paramagnetic shifts induced by nitroxide radicals in surrounding molecules depend on their interaction [7]. The most commonly studied nucleus for such analysis has been the ^{13}C nucleus [8–11]. The method of ^{13}C NMR of TEMPO-functionalized polymers has been used to study the thermoreversible phase transition of aqueous solutions of these polymers [12]. Effects have also been observed on the ^{1}H, ^{19}F, and ^{15}N nuclei [13]. The method of ^{1}H NMR was used to study the pressure effect on intermolecular interactions with nitroxide radicals [14].

Intermolecular interactions with nitroxide radicals can be characterized by studying their effect on the relaxation times of their diamagnetic partners [15–23]. The most definitive confirmation of complex formation between diamagnetic molecules and nitroxide radicals is the appearance of unpaired electron spin density on the nuclei of these molecules [24,25]. Nitroxide radicals act as proton acceptors, with hydrogen bonding being the most prominent mechanism for the formation of such complexes [26,27]. Complexes with alcohols [28–34], anilines [35,36], amines [24], acids [37,38], water [39], and phenols [40,41] are among the best studied.

On the other hand, intermolecular interactions cause two characteristic spectral changes in the nitroxide radicals themselves. These interactions manifest in changes in the isotropic hyperfine coupling constant $A_{iso}(^{14}N)$ [42,43] and variations in the relative linewidths of the components of the radical EPR signal. This difference in linewidth depends on the rate of rotational diffusion of the radical and can be used to study the physical properties of viscous liquids [44], ionic liquids [45,46], polymers [47], micelles [48,49], and inclusion complexes [50].

All the above parameters can be used either individually or in combination when utilizing radicals as probes to study complex molecular systems. However, in this publication, only the effect of molecular complexation on $A_{iso}(^{14}N)$ will be considered and discussed. This parameter is easy to measure, and, apparently, its changes are detectable even in cases of weak and transient interactions [51]. $A_{iso}(^{14}N)$ can be used to analyze steric effects on the accessibility of active sites [52–56] in a wide variety of weak proton donors and local micropolarity [57,58]. Such an analysis may provide a better understanding of the factors affecting the reactivity of these centers, whether through intramolecular interactions [59,60] or external influences [61,62]. Other studies [63,64] suggest that $A_{iso}(^{14}N)$ can also serve as a sensor for halogen bond properties [65,66].

The objectives of this study are as follows: (i) to identify a density functional theory (DFT) functional/basis set pair that accurately reproduces the experimental values of $A_{iso}(^{14}N)$ in aprotic solvents, which will then be used to interpret $A_{iso}(^{14}N)$ observed experimentally (ii) in water and alcohols, and (iii) in toluene solutions of phenols; (iv) to theoretically estimate the maximum possible value of $A_{iso}(^{14}N)$; and (v) to theoretically estimate the effect of halogen bonds on $A_{iso}(^{14}N)$. The radical (2,2,6,6-Tetramethylpiperidin-1-yl)oxyl (TEMPO) will be used as the model nitroxide radical. Figure 1 shows the molecular structure of this stable radical and its EPR spectrum in toluene. Wherever possible, calculated $A_{iso}(^{14}N)$ values are compared with the corresponding experimental values available in the literature.

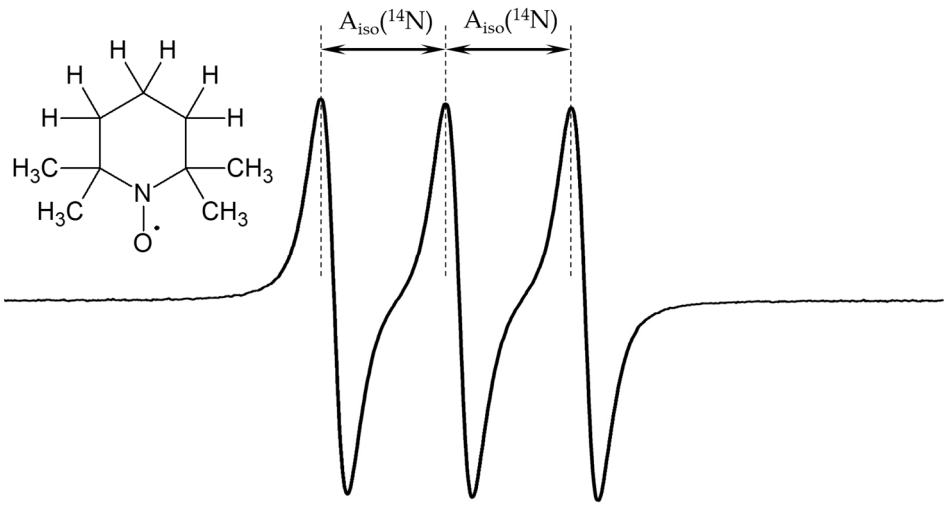

Figure 1. EPR spectrum of 5×10^{-4} M (2,2,6,6-Tetramethylpiperidin-1-yl)oxyl (TEMPO) in toluene at 300 K. $A_{iso}(^{14}N)$ = 1.55 mT, g = 2.0023.

2. Results and Discussion

2.1. The Best Functional/Basis Set Pair for Calculating $A_{iso}(^{14}N)$

Different DFT functional/basis set pairs have been tested in the past for calculations related to radicals. [67–69]. Here, several DFT functionals and basis sets were evaluated to calculate $A_{iso}(^{14}N)$ for TEMPO in toluene. Both the geometry of TEMPO and its $A_{iso}(^{14}N)$ were calculated using the polarizable continuum model approximation (PCM) with SCRF=(Solvent=toluene). The observed experimental value of $A_{iso}(^{14}N)$ decreases with increasing radical concentration [35,70]. Therefore, reliable calculated values of $A_{iso}(^{14}N)$ should equal or exceed the experimental value. Table 1 reports the calculated values of $A_{iso}(^{14}N)$ for selected DFT functional/basis set pairs.

The uPBE1PBE/LanL2DZ, uHSEH1PBE/LanL2DZ, and uHSEH1PBE/LanL2DZ pairs give results that are very close to the experimental value of 1.551 mT. However, in all cases, the calculated values are slightly lower than the experimental value. A possible reason for this deviation is that the effect of the reaction field created by the polarization of the surrounding dielectric cannot be correctly modeled within the PCM approach [58,71].

This can be addressed using a fictitious external electric field [71–73]. However, since the required field strength is solvent-dependent and cannot be estimated a priori, further calculations will be performed using the PCM approximation. If this explanation is correct, then the deviation between the theoretical and experimental values should increase with increasing solvent polarity.

Table 1. $A_{iso}(^{14}N)$ for TEMPO in toluene calculated for selected DFT functional/basis set pairs.

DFT Functional	Basis Set	$A_{iso}(^{14}N)$, mT
—	—	1.551 ± 0.002 [1]
uPBE1PBE	LanL2DZ	1.5147
uPBE1PBE	LanL2DZdp	1.4802
uPBE1PBE	EPR-III	1.0214
uPBE1PBE	6-31G-J	1.0222
uPBE1PBE	def2tzvp	0.9477
uPBE1PBE	aug-cc-pVqZ	0.8147
uHSEH1PBE	LanL2DZ	1.5154
uB3LYP	LanL2DZ	1.4629
uTPSSh	LanL2DZ	1.4233
uwB97XD	LanL2DZ	1.4559
uM06	LanL2DZ	1.1013

[1] Experimental value [52].

2.2. Aprotic Solvents

Table 2 reports the available experimental values of $A_{iso}(^{14}N)$ for TEMPO in aprotic solvents. For some of these solvents, $A_{iso}(^{14}N)$ was calculated in the uPBE1PBE/LanL2D approximation. Both the geometry of TEMPO and its $A_{iso}(^{14}N)$ were calculated in the PCM approximation using the solvent under study. In most cases, the calculated values are lower than the experimental ones. However, the deviations are not significant. The obtained data do not enable one to confirm or refute the assumption above that the deviation between the theoretical and experimental values increases with increasing solvent polarity. Nevertheless, the calculations correctly reproduce the trend for $A_{iso}(^{14}N)$ to increase with increasing solvent polarity. Notably, these changes are substantial enough to track even small variations in polarity. The experimental measurement error is on the order of 0.001 mT, and the absolute value changes by 0.1 mT when transitioning from hexane to (methanesulfinyl)methane (DMSO).

Table 2. $A_{iso}(^{14}N)$ for TEMPO in aprotic solvents.

Solvent	uPBE1PBE/LanL2DZ, mT	Experiment, mT
Hexane ($\varepsilon \approx 1.88$)	1.4996	1.520 [70] 1.50 [74]
Cyclohexane ($\varepsilon \approx 2.02$)	1.5042	1.540 [70] 1.51 [74]
CCl_4 ($\varepsilon \approx 2.23$)	1.5107	1.563 [75] 1.550 [70] 1.568 [35]
Benzene ($\varepsilon \approx 2.27$)	—	1.554 [76]
Toluene ($\varepsilon \approx 2.37$)	1.5147	1.551 [52]
Oxolane (THF, $\varepsilon \approx 7.43$)	1.5671	1.557 [77]
Dichloromethane ($\varepsilon \approx 8.93$)	—	1.587 [78]
DMSO ($\varepsilon \approx 46.83$)	1.5959	—
Ionic Liquid	—	1.604 [46]
Liquid CO_2	—	1.549 [79]
Supercritical CO_2	—	1.545 [79]
Mineral oil	—	1.539 [46]

2.3. Protic Solvents

Table 3 reports the available experimental values of $A_{iso}(^{14}N)$ for TEMPO in protic solvents. For some of these solvents, $A_{iso}(^{14}N)$ in 1:1 complexes of TEMPO and a solvent molecule was calculated in the uPBE1PBE/LanL2D approximation. Both the geometry of the complexes and $A_{iso}(^{14}N)$ were calculated in the PCM approximation using the solvent under study. The structures of some of these complexes are shown in Figure 2.

Table 3. $A_{iso}(^{14}N)$ in 1:1 complexes of TEMPO and selected solvent molecules.

Hydrogen Bond Donor	uPBE1PBE/LanL2DZ, mT	Experiment, mT
2-methylpropan-2-ol [1]	1.7108	1.60 [74]
Pentan-1-ol	—	1.61 [74]
3-methylbutan-1-ol	—	1.61 [74]
2-methylbutan-2-ol	—	1.58 [74]
Butan-2-ol	1.7256	1.60 [74]
Butan-1-ol	—	1.61 [74]
Propan-2-ol	—	1.61 [74]
Propan-1-ol	—	1.62 [74]
Ethanol	1.7337	1.632 [77] 1.62 [74]
Methanol [1]	1.7371	1.63 [74]
Water [1]	1.7274	1.769 [44] 1.732 [75]

[1] $A_{iso}(^{14}N)$ for TEMPO, calculated using the PCM approximation at ε = 78.36 (water), ε = 32.61 (methanol), and ε = 12.47 (2-methylpropan-2-ol), are 1.5984 mT, 1.5933 mT, and 1.5802 mT, respectively.

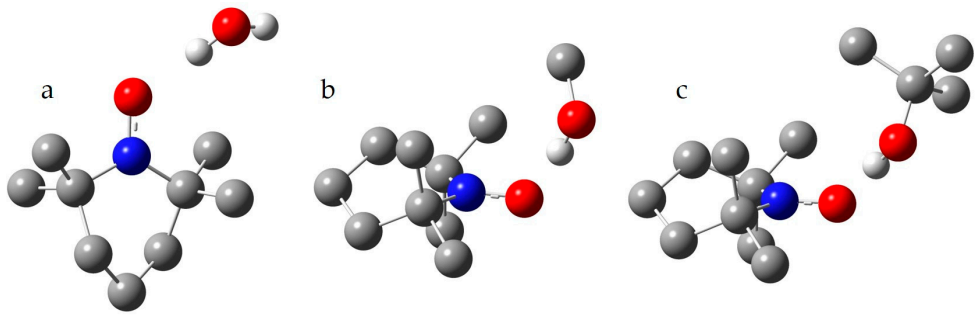

Figure 2. The model structures of the selected 1:1 complexes of TEMPO with (**a**) water, (**b**) methanol, and (**c**) 2-methylpropan-2-ol. Oxygen atoms are represented in red, nitrogen atoms in blue, carbon atoms in grey, and exchangeable protons in white.

Figure 2a shows the structure of the complex with a water molecule. The calculated $A_{iso}(^{14}N)$ value is lower than the experimental $A_{iso}(^{14}N)$ value in water. There are several possible reasons for this. First, the effect of the reaction field created by the polarization of the surrounding dielectric cannot be correctly modeled within the PCM approach [71–73]. Second, the proton-donating ability of a water molecule in water is greater than that of a single water molecule [80]. Given these limitations, the calculation result can be considered satisfactory and unequivocally indicates that the oxygen atom of TEMPO is involved in the hydrogen bond network of water. Note that the calculated $A_{iso}(^{14}N)$ value in the PCM SCRF=(solvent=water) approximation is only 1.5984 mT. Therefore, the hydrogen bond leads to an increase in $A_{iso}(^{14}N)$ by more than 0.12 mT.

Figure 2b,c shows the structures of two 1:1 complexes of TEMPO with alcohol molecules. For all studied alcohols, the calculated $A_{iso}(^{14}N)$ values in such complexes are similar to those with water but significantly exceed the available experimental values of $A_{iso}(^{14}N)$ in these alcohols, as seen in Table 3. On the other hand, these experimental values significantly exceed the calculated $A_{iso}(^{14}N)$ values in the PCM SCRF=(solvent=alcohol) approximation. The hydrogen bonds in these 1:1 complexes lead to an increase in $A_{iso}(^{14}N)$ by more than 0.13 mT. The observed difference between the calculated and experimental values indicates that in alcohols, TEMPO may or may not be hydrogen-bonded. Greatly simplifying the

real situation and assuming that there is an equilibrium between TEMPO molecules that do not participate in any way in hydrogen bonding and TEMPO molecules forming the 1:1 complexes of optimal geometry with the alcohol molecules, one can write the following: $A_{iso}(^{14}N)^{exp} = x_H \cdot A_{iso}(^{14}N)^{H} + x_f \cdot A_{iso}(^{14}N)^{f}$, where $A_{iso}(^{14}N)^{exp}$, $A_{iso}(^{14}N)^{H}$, and $A_{iso}(^{14}N)^{f}$ stand for the observed experimental value, the calculated value in the 1:1 complex, and the calculated value for TEMPO in the PCM approximation, respectively. x_H and x_f are the mole fractions of the hydrogen-bonded and free TEMPO molecules, respectively, and $x_H + x_f = 1$. Thus, $x_H = (A_{iso}(^{14}N)^{exp} - A_{iso}(^{14}N)^{f})/(A_{iso}(^{14}N)^{H} - A_{iso}(^{14}N)^{f})$. For TEMPO in methanol, $x_H = (1.63 - 1.5933)/(1.7371 - 1.5933) \approx 0.25$. For TEMPO in 2-methylpropan-2-ol, $x_H \approx 0.15$. Of course, these mole fractions must largely depend on the proton-donating ability of the alcohol molecule and the temperature.

2.4. Interaction of TEMPO with Phenols in Toluene

Table 4 presents the available experimental values of $A_{iso}(^{14}N)$ for TEMPO in solutions of phenols in toluene. For some of these phenols, $A_{iso}(^{14}N)$ in 1:1 complexes of TEMPO and a phenol molecule was calculated in the uPBE1PBE/LanL2D approximation. Both the geometry of the complexes and $A_{iso}(^{14}N)$ were calculated in the PCM approximation in toluene. The structures of these complexes are shown in Figure 3.

Table 4. $A_{iso}(^{14}N)$ for TEMPO in 1:1 complexes with phenols in toluene. [1] The experimental values were obtained for TEMPO/phenol concentrations of 5×10^{-4} M/0.01 M and 5×10^{-4} M/0.05 M.

Phenol	uPBE1PBE/LanL2DZ, mT	Experiment [52], mT	
		0.01 M	0.05 M
Phenol	1.7415	1.565	1.607
4-nitrophenol	1.7852	1.595	1.633
2,5-dinitrophenol	1.8023	1.556	1.574
2,4,6-trinitrophenol	1.6242	1.552	1.557
2,6-di-*tert*-butylphenol	—	1.552	1.554

[1] The experimental and calculated $A_{iso}(^{14}N)$ values for TEMPO in toluene are 1.551 mT [52] and 1.5147 mT, respectively.

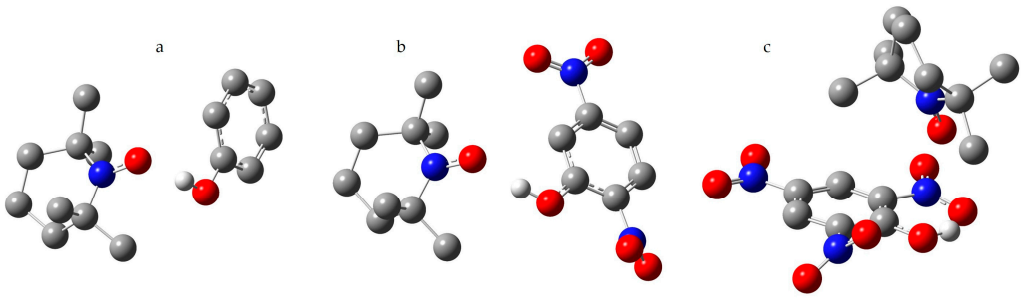

Figure 3. The model structures of the 1:1 complexes of TEMPO with (**a**) phenol, (**b**) 2,5-dinitrophenol, and (**c**) 2,4,6-trinitrophenol. Oxygen atoms are represented in red, nitrogen atoms in blue, carbon atoms in grey, and exchangeable protons in white.

Phenol and 4-nitrophenol form with TEMPO hydrogen-bonded complexes, as seen in Figure 3a. The mole fractions of these complexes in the studied solution can be estimated using $x_H = (A_{iso}(^{14}N)^{exp} - A_{iso}(^{14}N)^{Tol})/(A_{iso}(^{14}N)^{H} - A_{iso}(^{14}N)^{Tol})$, where $A_{iso}(^{14}N)^{Tol}$ stands for the experimental value in toluene, 1.551 mT [52]. x_H depends on the phenol concentration. For concentrations of 0.01 M and 0.05 M, x_H is approximately 0.07 and 0.29 for phenol and 0.19 and 0.35 for 4-nitrophenol, respectively.

The hydrogen bond with 2,5-dinitrophenol should be even stronger, as seen in Table 4 and Figure 3b. However, the estimated values of x_H are only about 0.02 and 0.09 for concentrations 0.01 M and 0.05 M, respectively. This indicates that the presence of a nitro group in the *ortho* position greatly hinders the formation of the complex. If both *ortho*

positions are occupied by nitro groups, 2,4,6-trinitrophenol, the hydroxyl group prefers to form an intramolecular hydrogen bond with one of them, as seen in Figure 3c. The calculated value of $A_{iso}(^{14}N)$ in such a complex is low, as seen in Table 4. The absence of hydrogen bonding between 2,4,6-trinitrophenol and TEMPO in toluene is also confirmed by the low experimental value of $A_{iso}(^{14}N)$. The same is true for 2,6-di-*tert*-butylphenol, as seen in Table 4. Therefore, *tert*-butyl groups at the *ortho* positions block the proton-donating ability of phenol just as they block the proton-accepting ability of pyridine [81].

Note that with a 5-fold increase in phenol concentration, the increase in x_H values depends on the type of phenol. For phenol, x_H increases 4-fold, for 4-nitrophenol it doubles, and for 2,5-dinitrophenol, it increases 5-fold. One can speculate that these changes reflect the instantaneous concentration of the TEMPO/phenol hydrogen-bonded complexes of different geometry in solutions at phenol concentrations of 0.01 M. Phenol is a weak proton donor, resulting in short lifetimes for its hydrogen-bonded complexes at room temperature. Consequently, most TEMPO molecules remain free when the phenol concentration is low. 2,5-dinitrophenol is a stronger proton donor, but the lifetime of its hydrogen-bonded complexes is limited by steric interference from its ortho substituent. Therefore, most TEMPO molecules remain free in this case, as well when phenol concentration is low. For both phenols, the energy gain from hydrogen bonding is offset by entropy losses. When most TEMPO molecules in solution remain free, a 5-fold increase in phenol concentration leads to a 5-fold increase in the concentration of short-living hydrogen-bonded complexes. In contrast, 4-nitrophenol is a strong proton donor with no steric hindrances to its hydrogen bonding, so the instantaneous concentration of TEMPO/4-nitrophenol hydrogen-bonded complexes is already significant at a phenol concentration of 0.01 M. In this case, an increase in the phenol concentration causes only a limited increase in the instantaneous concentration of the hydrogen-bonded complexes.

2.5. Interaction of TEMPO with Strong Proton Donors

What is the largest possible value for $A_{iso}(^{14}N)$ of TEMPO? The largest experimentally measured values are around 2.18−2.19 mT [76,78], attributed to TEMPO-H^+. Strong acids can cause chemical degradation of the nitroxide paramagnetic center [82–85], so the actual existence of the complexes discussed below cannot be confirmed here. The current goal is to estimate the Aiso(^{14}N) values that can be expected for complexes between TEMPO and strong proton donors.

The calculated $A_{iso}(^{14}N)$ value for the TEMPO-H^+ cation is 2.42 mT, as seen in Table 5, with both its geometry and $A_{iso}(^{14}N)$ value calculated using the PCM approximation in water. The orientation of proton donors relative to the N-O$^\bullet$ moiety of TEMPO, as shown in Figures 2 and 3, suggests that its proton-accepting ability may be similar to the P=O moiety. This allows for the simultaneous formation of two hydrogen bonds of equal energy [86,87]. This feature of the P=O moiety significantly influences the structure of its hydrogen-bonded adducts [88–92]. The calculated $A_{iso}(^{14}N)$ for the TEMPO-$2H^{2+}$ cation is 2.45 mT, as seen in Table 5. Both its geometry and $A_{iso}(^{14}N)$ value were calculated using the PCM approximation in water.

Table 5. The calculated $A_{iso}(^{14}N)$ values of TEMPO in mT in complexes with selected proton donors.

Hydrogen-Bonded Complex	uPBE1PBE/LanL2DZ	O. . .H Distance, Å
TEMPO-H^+ in water	2.4242 [1]	0.97
TEMPO-$2H^{2+}$ in water	2.4540 [1]	0.99
TEMPO-HF in water	1.8508 [1]	1.53
TEMPO-2HF in water	2.0509 [1]	1.59
TEMPO-[H-pyridine]$^+$ in toluene	1.8620 [2]	1.61
TEMPO-[H-BiPy]$^+$ in toluene	1.7468 [2]	1.87
TEMPO-[H-Phen]$^+$ in toluene	1.8145 [2]	1.71

[1] The calculated $A_{iso}(^{14}N)$ value of TEMPO in water is 1.5984 mT. [2] The calculated $A_{iso}(^{14}N)$ value of TEMPO in toluene is 1.5147 mT.

To analyze the difference between TEMPO adducts with one and two hydrogen bond donors, its complexes with hydrogen fluoride (HF) were examined. Figure 4a,b shows their structures. Both the geometry of these adducts and their $A_{iso}(^{14}N)$ value were calculated using the PCM approximation in water. Unlike the TEMPO cations discussed earlier, there is a significant difference in $A_{iso}(^{14}N)$ for these adducts, as seen in Table 5. The formation of the second hydrogen bond in the TEMPO. . .2HF adduct leads to a lengthening of the O. . .H distances. Is the formation of two hydrogen bonds energetically favorable? The hydrogen bond energy in these adducts can be defined as the difference between (i) the sum of the electronic energies of a noninteracting TEMPO molecule and one or two noninteracting HF molecules, and (ii) the electronic energy of the TEMPO. . .HF or TEMPO. . .2HF adducts, all calculated using the PCM approximation in water. For the TEMPO. . .HF adduct, the hydrogen bond energy is 49 kJ/mol, while for the TEMPO. . .2HF adduct, it is 87 kJ/mol $\approx 2 \times 44$ kJ/mol. Therefore, similar to the P=O moiety, the N-O$^{\bullet}$ moiety in TEMPO can form two equally strong hydrogen bonds simultaneously.

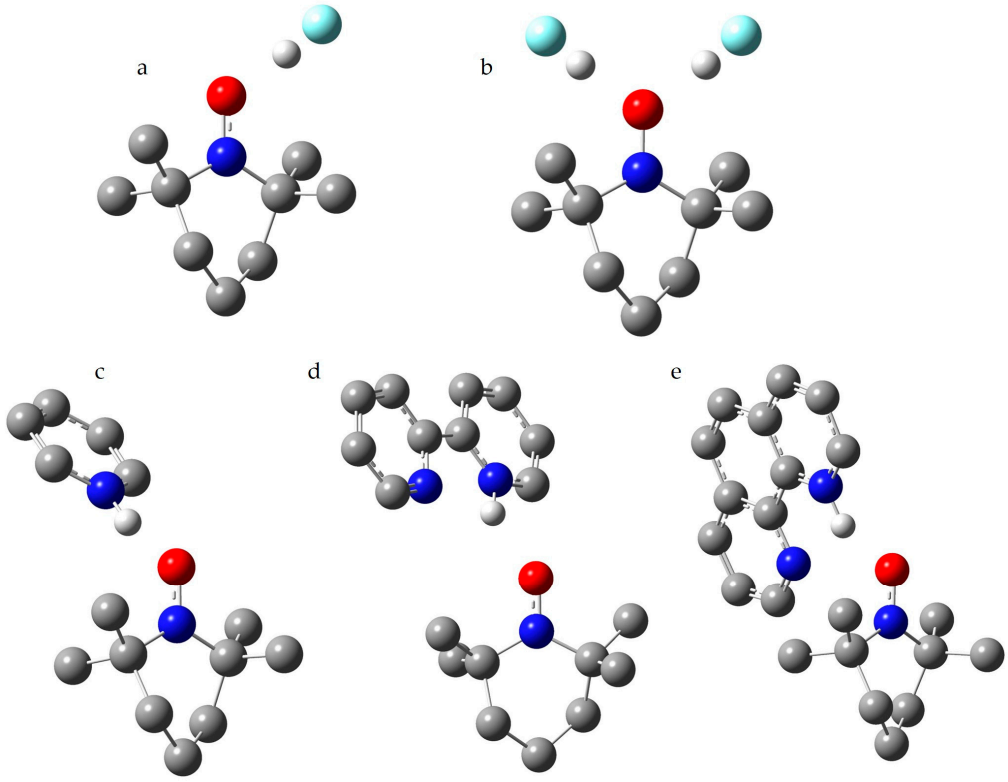

Figure 4. The model structures of the complexes of TEMPO with strong proton donors. (**a**) Hydrogen fluoride. (**b**) Two molecules of hydrogen fluoride. (**c**) Pyridine-H$^+$ cation. (**d**) 2,2′-bipyridine-H$^+$ cation. (**e**) 1,10-phenanthroline-H$^+$ cation. Oxygen atoms are represented in red, nitrogen atoms in blue, carbon atoms in grey, fluorine atoms in cyan, and exchangeable protons in white.

This has important implications: in water and other protic solvents, adducts with two hydrogen bonds per TEMPO molecule are likely to exist. $A_{iso}(^{14}N)$ in these adducts is larger than in 1:1 adducts. This may be another reason why the experimental $A_{iso}(^{14}N)$ in water is greater than the calculated value for the 1:1 complex, as seen in Table 3. It also implies that the actual concentration of hydrogen-bonded TEMPO forms in alcohols is lower than what is estimated from the calculated $A_{iso}(^{14}N)$ for 1:1 complexes.

Figure 4c shows the structure of the 1:1 complex of TEMPO with the pyridine-H$^+$ cation. Both the geometry and $A_{iso}(^{14}N)$ value were calculated using the PCM approximation in toluene. This cation is a stronger proton donor than alcohols and phenols. As a result, the hydrogen bond in this complex leads to an increase in the $A_{iso}(^{14}N)$ value by more than 0.3 mT, as seen in Table 5. The presence of such complexes in solution should

be easy to detect. The O. . .H distance in this complex is similar to the O. . .H distances in pyridine complexes with benzoic acid dimers [93]. However, the formation of the 1:2 adducts discussed earlier cannot be ruled out. In experimental studies of such systems, a balance must be struck between competing factors: the solvent must be sufficiently inert so as not to compete with the cation for interaction with TEMPO, while still maintaining sufficient solubility of the cation.

The *cis*-conformation of the 2,2′-bipyridine-H^+ ($[H\text{-}BiPy]^+$) cation is stabilized by a weak intramolecular hydrogen bond [94]. This bond plays a critical role in facilitating a reversible intramolecular proton transfer [95]. Figure 4d,e shows the structures of the 1:1 complexes of TEMPO with $[H\text{-}BiPy]^+$ and $[H\text{-}Phen]^+$. Both the geometry and $A_{iso}(^{14}N)$ value were calculated using the PCM approximation in toluene. The significant differences in $A_{iso}(^{14}N)$ and the O. . .H distances in these complexes are likely attributed to the effect of TEMPO on their intramolecular bonds, as seen in Table 5. In $[H\text{-}Phen]^+$, this effect appears to be more pronounced compared to $[H\text{-}BiPy]^+$. Nevertheless, the changes in $A_{iso}(^{14}N)$ should be readily detectable experimentally for both complexes. It would be instructive to experimentally investigate whether a weak interaction with TEMPO can influence the energy balance in $[H\text{-}BiPy]^+$ and alter its conformation from *cis* to *trans*.

2.6. Interaction of TEMPO with a Strong Halogen Bond Donor

Figure 5 shows the structure of the 1:1 complex of TEMPO with iodo 2,2,2-trifluoroacetate. Both the geometry and $A_{iso}(^{14}N)$ value were calculated using the PCM approximation in hexane. The choice of such a strong halogen bond donor [96] and a low polarity solvent was made deliberately to evaluate the maximum changes in $A_{iso}(^{14}N)$ expected for halogen bonding. The calculated $A_{iso}(^{14}N)$ value of TEMPO in hexane, equal to 1.4996 mT, increases to 1.8635 mT in this complex. The presence of such complexes in solution should be easily detected, even if their mole fraction is low.

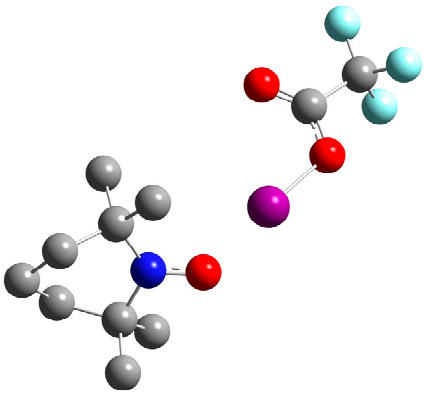

Figure 5. The model structure of the 1:1 complexes of TEMPO with iodo 2,2,2-trifluoroacetate in hexane. The calculated $A_{iso}(^{14}N)$ value in this complex is 1.8635 mT. The calculated $A_{iso}(^{14}N)$ value of TEMPO in hexane is 1.4996 mT. Oxygen atoms are represented in red, the nitrogen atom in blue, carbon atoms in grey, and the iodine atom in purple.

3. Materials and Methods

The Gaussian 09.D.01 program package was used for geometry optimizations and EPR calculations [97], employing the ωB97XD/def2tzvp and uPBE1PBE/LanL2DZ DFT functional/basis set pairs, respectively [98–101]. The optimized geometries and the results of selected EPR calculations are reported in the Supplementary Materials. All calculations were performed using the PCM approximation. Although the results of such calculations are not highly sensitive to the specific value of the dielectric constant, applying this correction is important to account for the effects of the surrounding medium [102]. This study does not address whether other solvent models, such as the Solvation Model based on Density (SMD), the Conductor-like Polarizable Continuum Model (CPCM), or the Conductor-like Screening Model (COSMO), provide better approximations for medium

effects. There is no reason to expect that TEMPO is a particularly convenient model system for answering this question. It is quite possible that when using one of these models, the uPBE1PBE/LanL2DZ DFT functional/basis set pair will no longer be the most suitable for EPR calculations. However, a more suitable pair can be easily found for the solvent model in question using the approach outlined in Table 1.

4. Conclusions

The isotropic hyperfine coupling constant $A_{iso}(^{14}N)$ of the stable nitroxide radical TEMPO can be measured experimentally with an accuracy of 0.001 mT. The variation in this constant due solely to the polarity of the solvent is about 0.1 mT. The variations due to halogen and hydrogen bonding are greater than 0.3 mT and 0.5 mT, respectively. Therefore, $A_{iso}(^{14}N)$ serves as a highly sensitive experimental probe for detecting the effects of the surrounding medium and non-covalent interactions.

$A_{iso}(^{14}N)$ can be calculated for model systems of required complexity with reasonable accuracy using the uPBE1PBE/LanL2DZ approximation, which requires only moderate computational effort. If higher accuracy is desired, more sophisticated methods can be employed [103].

However, the most challenging aspect of such calculations is not the accuracy of the computational method but accounting for the effects of the surrounding medium and the presence of a variety of non-covalently bound complexes in solution, with diverse compositions and geometries. Each of these complexes exhibits a different $A_{iso}(^{14}N)$ value. The structure and linewidth of the experimental spectrum depend on the relative concentration of these complexes, their lifetimes, and their tumbling times. If a study does not involve frozen solutions [104–106], interpreting the experimental spectra in terms of the structure and geometry of the potential complexes will require evaluating numerous model structures, the relative average concentration of which, in solution, cannot always be reliably predicted based on general assumptions [107]. Ideally, additional experimental measurements at very low concentrations should also be performed. In any case, for TEMPO, the list of possible model structures must include complexes featuring two conjugated hydrogen bonds.

This work examines the influence of various non-covalent interactions on $A_{iso}(^{14}N)$ without a thorough analysis of the changes in the electron density distribution caused by these interactions, which, in turn, determines the observed changes in the $A_{iso}(^{14}N)$ value. However, conducting such an analysis at a reliable level would require a separate, specialized study based on the implementation of appropriate experimental studies. Such studies are beyond the scope of this paper, although the results obtained here can help in planning the practical part of such studies.

Supplementary Materials: The following supporting information can be downloaded at: https://www.mdpi.com/article/10.3390/molecules29215032/s1, Table S1: The optimized molecular structure of TEMPO in toluene; Table S2: The optimized molecular structure of TEMPO in DMSO; Table S3: The optimized molecular structure of TEMPO in n-Hexane; Table S4: The optimized molecular structure of 1:1 complex of TEMPO and water; Table S5: The optimized molecular structure of 1:1 complex of TEMPO and methanol; Table S6: The optimized molecular structure of 1:1 complex of TEMPO and ethanol; Table S7: The optimized molecular structure of 1:1 complex of TEMPO and Butan-2-ol; Table S8: The optimized molecular structure of 1:1 complex of TEMPO and 2-methylpropan-2-ol; Table S9: The optimized molecular structure of 1:1 complex of TEMPO and phenol; Table S10: The optimized molecular structure of 1:1 complex of TEMPO and 4-nitrophenol; Table S11: The optimized molecular structure of 1:1 complex of TEMPO and 2,5-dinitrophenol; Table S12: The optimized molecular structure of 1:1 complex of TEMPO and 2,4,6-trinitrophenol; Table S13: The optimized molecular structure of $[TEMPO\text{-}H]^+$; Table S14: The optimized molecular structure of $[TEMPO\text{-}2H]^{2+}$; Table S15: The optimized molecular structure of 1:1 complex of TEMPO and HF; Table S16: The optimized molecular structure of 1:2 complex of TEMPO and HF; Table S17: The optimized molecular structure of 1:1 complex of TEMPO and $[H\text{-pyridine}]^+$; Table S18: The optimized molecular structure of 1:1 complex of TEMPO and $[H\text{-BiPy}]^+$; Table S19: The optimized molecular structure of 1:1 complex

of TEMPO and [H-Phen]$^+$; Table S20: The optimized molecular structure of 1:1 complex of TEMPO and iodo 2,2,2-trifluoroacetate; Table S21: The isotropic Fermi contact couplings in TEMPO in toluene; Table S22: The isotropic Fermi contact couplings in TEMPO in DMSO; Table S23: The isotropic Fermi contact couplings in TEMPO in n-hexane; and Table S24: The isotropic Fermi contact couplings in 1:1 complex of TEMPO and water.

Funding: This research received no external funding.

Institutional Review Board Statement: Not applicable.

Informed Consent Statement: Not applicable.

Data Availability Statement: Data are contained within the article and Supplementary Materials.

Acknowledgments: The author thanks Anton Savitsky for assistance with the literature searches and motivation to write this article, and Gábor Balázs for help with conducting model EPR measurements.

Conflicts of Interest: The author declares no conflict of interest.

References

1. Vega, S. Dynamic Nuclear Polarization with or without Spin Diffusion? *Online Lect.* 2011. Available online: https://www.youtube.com/watch?v=-7xu7a0YQy4 (accessed on 7 October 2024).
2. Asanbaeva, N.B.; Dobrynin, S.A.; Morozov, D.A.; Haro-Mares, N.; Gutmann, T.; Buntkowsky, G.; Bagryanskaya, E.G. An EPR Study on Highly Stable Nitroxyl-Nitroxyl Biradicals for Dynamic Nuclear Polarization Applications at High Magnetic Fields. *Molecules* **2023**, *28*, 1926. [CrossRef] [PubMed]
3. Herr, K.; Fleckenstein, M.; Brodrecht, M.; Höfler, M.V.; Heise, H.; Aussenac, F.; Gutmann, T.; Reggelin, M.; Buntkowsky, G. A novel strategy for site selective spin-labeling to investigate bioactive entities by DNP and EPR spectroscopy. *Sci. Rep.* **2021**, *11*, 13714. [CrossRef] [PubMed]
4. van der Heijden, G.H.A.; Kentgens, A.P.M.; van Bentum, P.J.M. Liquid state dynamic nuclear polarization of ethanol at 3.4 T (95 GHz). *Phys. Chem. Chem. Phys.* **2014**, *16*, 8493–8502. [CrossRef] [PubMed]
5. Russ, J.L.; Gu, J.; Tsai, K.-H.; Glass, T.; Duchamp, J.C.; Dorn, H.C. Nitroxide/Substrate Weak Hydrogen Bonding: Attitude and Dynamics of Collisions in Solution. *J. Am. Chem. Soc.* **2007**, *129*, 7018–7027. [CrossRef] [PubMed]
6. Sert, I.; Sünnetçioğlu, M.M.; Sungur, R.; Bingöl, G. Dynamic Nuclear Polarization Studies of TANOL/water-glycerol Solutions. *Z. Für Naturforschung A* **2000**, *55*, 682–686. [CrossRef]
7. Waterton, J.C.; Sanders, J.K.M. Radical-induced pseudocontact shifts. *J. Am. Chem. Soc.* **1978**, *100*, 1295–1296. [CrossRef]
8. Qiu, Z.W.; Grant, D.M.; Pugmire, R.J. Paramagnetic Carbon- 13 Shifts Induced by the Free Radical 2,2,6,6-Tetramethylpiperidinyl-1-oxy. 1. Simple Aromatic and Paraffinic Hydrocarbons. *J. Am. Chem. Soc.* **1982**, *104*, 2747–2753. [CrossRef]
9. Qiu, Z.W.; Grant, D.M.; Pugmire, R.J. Paramagnetic carbon-13 shifts induced by the free radical Tempo. 2. Nitrogen heterocycles. *J. Am. Chem. Soc.* **1984**, *106*, 557–563. [CrossRef]
10. Sysoeva, N.A.; Pekhk, T.I.; Lippmaa, É.T.; Buchachenko, A.L. NMR in paramagnetic radical complexes with organic ligands. III. Paramagnetic shifts of C^{13}. *J. Struct. Chem.* **1972**, *13*, 392–395. [CrossRef]
11. Draney, D.; Kingsbury, C.A. Free radical induced nuclear magnetic resonance shifts: Comments on contact shift mechanisms. *J. Am. Chem. Soc.* **1981**, *103*, 1041–1047. [CrossRef]
12. Winnik, F.M.; Ottaviani, M.F.; Bossman, S.H.; Pan, W.; Garcia-Garibay, M.; Turro, N.J. Phase separation of poly (N-isopropylacrylamide) in water: A spectroscopic study of a polymer tagged with a fluorescent dye and a spin label. *J. Phys. Chem.* **1993**, *97*, 12998–13005. [CrossRef]
13. Wawer, I.; Ströhl, D.; Kleinpeter, E. Nitroxide radical as a probe for molecular conformation. Part I. ^{13}C NMR study of the interaction of N,N-dimethylamides with nitroxide radical. *Magn. Reason. Chem.* **1993**, *31*, 758–762. [CrossRef]
14. Endo, K.; Hazama, Y.; Okabayashi, K.; Tonoike, I.; Suzuki, K. Pressure dependence of NMR spectroscopy for studying intermolecular interactions ^{1}H NMR in organic solvents involving the nitroxide radical. *Chem. Phys. Lett.* **1979**, *61*, 336–338. [CrossRef]
15. Sysoeva, N.A.; Buchachenko, A.L. NMR of paramagnetic complexes of radicals with organic ligands. I. Complexes with Zydroxyl-Containing Ligands. *J. Struct. Chem.* **1972**, *13*, 35–41. [CrossRef]
16. Sysoeva, N.A.; Buchachenko, A.L. NMR of paramagnetic complexes of radicals with organic ligands. I. Method of determination of lifetimes and distances in complexes. *Chem. Phys.* **1975**, *7*, 123–129. [CrossRef]
17. Sysoeva, N.A.; Karmilov, A.Y.; Buchachenko, A.L. NMR in paramagnetic complexes of radicals with organic ligands. II. Method of identification of electronic structure of complexes—Theory. *Chem. Phys.* **1976**, *15*, 313–319. [CrossRef]
18. Sysoeva, N.A.; Karmilov, A.Y.; Buchachenko, A.L. NMR in paramagnetic complexes of radicals with organic ligands: III. Method of identification of electronic structure of complexes—Experiment. *Chem. Phys.* **1976**, *15*, 321–330. [CrossRef]
19. Borah, B.; Bates, R.D., Jr. Interspecies hydrogen bonding between a nitroxide spin label and perfluoro-t-butanol studied by DNP and ^{1}H and ^{19}F relaxation measurements. *Chem. Phys. Lett.* **1980**, *76*, 101–104. [CrossRef]

20. Borah, B.; Bates, R.D., Jr. Dynamics of interspecies hydrogen bonding of a fluorinated alcohol and a nitroxide free radical. *J. Chem. Phys.* **1981**, *74*, 1538–1545. [CrossRef]
21. Bundfuss, K.; Meise-Gresch, K.; Müller-Warmuth, W. Hydrogen bond formation and molecular motion in solutions of chlorofluoromethanes containing nitroxide free radicals. *J. Magn. Res.* **1983**, *55*, 408–420. [CrossRef]
22. Darges, G.; Müller-Warmuth, W. NMR T_1 study of dipolar and scalar spectral densities for intermolecular relaxation in solutions of free radicals over a large frequency and temperature range. *J. Magn. Res.* **1985**, *65*, 444–458. [CrossRef]
23. Nientiedt, H.-W.; Bundfuss, K.; Müller-Warmuth, W. Frequency and temperature dependence of NMR relaxation for protic solvents with complexes of nitroxide radicals. *J. Magn. Res.* **1981**, *43*, 154–166. [CrossRef]
24. Sysoeva, N.A.; Stepanyants, A.U.; Buchachenko, A.L. Paramagentic shift of solvent protons in the presence of organic radicals. *J. Struct. Chem.* **1968**, *9*, 248–249. [CrossRef]
25. Sysoeva, N.A.; Buchachenko, A.L. NMR in complexes of radicals with organic ligands II. Amines, halogen-containing compounds and unsaturated compounds. *J. Struct. Chem.* **1972**, *13*, 205–208. [CrossRef]
26. Grabowski, S.J. What Is the Covalency of Hydrogen Bonding? *Chem. Rew.* **2011**, *111*, 2597–2625. [CrossRef]
27. Alkorta, I.; Rozas, I.; Elguero, J. Non-conventional hydrogen bonds. *Chem. Soc. Rev.* **1998**, *27*, 163170. [CrossRef]
28. Samitov, Y.Y.; Ibraimov, D. NMR study of molecular interaction in solutions of 2,2,6,6-tetramethylpentamethylenenitroxyl. *Theor. Exp. Chem.* **1965**, *1*, 251–254. [CrossRef]
29. Koodziejski, W.; Kęcki, Z. ^{13}C NMR study of alcohols complexed with nitroxide radical. *Chem. Phys. Lett.* **1978**, *54*, 286–288. [CrossRef]
30. Bonesteel, J.-A.K.; Borah, B.; Bates, R.D., Jr. Effects of nitroxide free radicals on proton donor chemical shifts. *J. Mang. Reason.* **1992**, *98*, 475–482. [CrossRef]
31. Dally, E.; Müller-Warmuth, W. NMR-Untersuchungen an Lösungen mit Nitroxidradikalkomplexen. II. Hyperfeinkopplungskonstanten, Linienbreiten und Relaxation von Komplexen mit n-Propanol, Isopropanol und tert.-Butanol. *Ber. Bunsenges. Phys. Chem.* **1978**, *82*, 792–798. [CrossRef]
32. Dally, E.; Müller-Warmuth, W. NMR-Untersuchungen an Lösungen mit Nitroxidradikalkomplexen. III. Komplexe mit Äthanol, Isoamylalkohol, n-Dekanol, Glykol, Cyclohexanol und Triäthylcarbinol. *Ber. Bunsenges. Phys. Chem.* **1980**, *84*, 260–265. [CrossRef]
33. Endo, K.; Morishima, I.; Yonezawa, T. Use of a stable free radical as a NMR spin probe for studying intermolecular interactions. XIV. A proton relaxation study of the hydrogen bond involving a stable free radical. *J. Chem. Phys.* **1977**, *67*, 4760–4767. [CrossRef]
34. Morishima, I.; Endo, K.; Yonezawa, T. Nuclear magnetic resonance contact shifts induced by hydrogen bonding with organic radicals. I. ^{1}H and ^{13}C contact shifts of protic molecules in the presence of the nitroxide radical. *J. Am. Chem. Soc.* **1971**, *93*, 2048–2050. [CrossRef]
35. Wawer, I.; Krysiak, T.; Kęcki, Z. NMR and EPR study of hydrogen bonding in chloroanilines. *J. Mol. Struct.* **1994**, *326*, 163–170. [CrossRef]
36. Stark, U.; Müller-Warmuth, W. Hydrogen Bond Formation and Molecular Motion in Solutions of Aniline with Nitroxide Free Radicals. *Ber. Bunsenges. Phys. Chem.* **1990**, *94*, 168–172. [CrossRef]
37. Dally, E.; Müller-Warmuth, W. Hochauflösende NMR an Lösungen mit Nitroxidradikalkomplexen. *Ber. Bunsenges. Phys. Chem.* **1977**, *81*, 1133–1137. [CrossRef]
38. Endo, K.; Knuettel, B.; Morishima, I.; Inubushi, T.; Yonezawa, T. Interaction between closed-shell and open-shell molecules. ^{1}H relaxation studies of the hydrogen bond between proton-donor molecules and a nitroxide radical. *Chem. Phys. Lett.* **1975**, *31*, 387–391. [CrossRef]
39. Meise, K.; Müller-Warmuth, W.; Nientiedt, H.-W. Magnetische Resonanzuntersuchungen zur Struktur, Kinetik und Hyperfeinwechselwirkung des Systems Nitroxidradikal-Wasser. *Ber. Bunsenges. Phys. Chem.* **1976**, *80*, 584–590. [CrossRef]
40. Pokhodenko, V.D.; Slipenyuk, T.S.; Kuts, V.S. Effect of the electronic structure of a diamagnetic molecule on the formation of complexes with free radicals. *Theor. Exp. Chem.* **1976**, *11*, 39–43. [CrossRef]
41. Cramer, R.E.; Dahlstrom, P.L.; Heya, H. Fluorine-19 and hydrogen contact shifts of Lewis acids hydrogen bonded to a stable free radical. Non-Curie law behavior. *J. Phys. Chem.* **1975**, *79*, 376–380. [CrossRef]
42. Hatch, G.F.; Kreilick, R.W. NMR of Some Nitroxide Radicals: ^{13}C Coupling Constants. *J. Chem. Phys.* **1972**, *57*, 3696–3699. [CrossRef]
43. Kuts, V.S.; Radchenko, N.F.; Pokhodenko, V.D. Electronic structure of free-nitroxide-radical—Aromatic-molecule π complexes. *Theor. Exp. Chem.* **1981**, *16*, 447–453. [CrossRef]
44. Milton Franklin Benial, A.; Kumara Dhas, M.; Jawahar, A. Rotational Correlation Time Studies on Nitroxyl Radicals Using 300 MHz ESR Spectrometer in High Viscous Liquid. *Appl. Magn. Reason.* **2011**, *40*, 311–319. [CrossRef]
45. Strehmel, V.; Berdzinski, S.; Rexhausen, H. Interactions between ionic liquids and radicals. *J. Mol. Liq.* **2014**, *192*, 153–170. [CrossRef]
46. Noël, M.A.M.; Allendoerfer, R.D.; Osteryoung, R.A. Solvation in Ionic Liquids: An EPR Study. *J. Phys. Chem.* **1992**, *96*, 2391–2394. [CrossRef]
47. Švajdlenková, H.; Šauša, O.; Adichtchev, S.V.; Surovtsev, N.V.; Novikov, V.N.; Bartoš, J. On the Mutual Relationships between Molecular Probe Mobility and Free Volume and Polymer Dynamics in Organic Glass Formers: Cis-1,4-poly(isoprene). *Polymers* **2021**, *13*, 294. [CrossRef]

48. Walski, T.; Gałecka, T.; Grzeszczuk-Kuć, K.; Komorowska, M. Modification of the hydrogen bonding network at the reversed micelles interface by near infrared radiation. *Nukleonika* **2013**, *58*, 435–438. Available online: https://yadda.icm.edu.pl/baztech/element/bwmeta1.element.baztech-4e16d03d-8cc6-4fef-b50e-d6b60865d291/c/Modification_of_the_hydrogen_bonding_network.pdf (accessed on 30 June 2023).
49. Tedeschi, A.M.; D'Errico, G.; Busi, E.; Basosi, R.; Barone, V. Micellar aggregation of sulfonate surfactants studied by electron paramagnetic resonance of a cationic nitroxide: An experimental and computational approach. *Phys. Chem. Chem. Phys.* **2002**, *4*, 2180–2188. [CrossRef]
50. Liu, F.; Karoui, H.; Rockenbauer, A.; Liu, S.; Ouari, O.; Bardelang, D. EPR Spectroscopy: A Powerful Tool to Analyze Supramolecular Host•Guest Complexes of Stable Radicals with Cucurbiturils. *Molecules* **2020**, *25*, 776. [CrossRef]
51. Griffith, O.H.; Dehlinger, P.J.; Van, S.P. Shape of the hydrophobic barrier of phospholipid bilayers (Evidence for water penetration in biological membranes). *J. Membrain Biol.* **1974**, *15*, 159–192. [CrossRef]
52. Shenderovich, I.G.; Wawer, I.; Denisov, G.S.; Kecki, Z. NMR and EPR study of the nitroxide radical TEMPO interaction with phenols. *Spectrosc. Lett.* **1997**, *30*, 1515–1523. [CrossRef]
53. Kuts, V.S.; Slipenyuk, T.S.; Pokhodenko, V.D. Effect of the steric structure of molecules on complex formation in the free radical -2,6-dialkylphenol system. *Theor. Exp. Chem.* **1976**, *12*, 614–619. [CrossRef]
54. Kuts, V.S.; Slipenyuk, T.S.; Platonova, É.P.; Pokhodenko, V.D. Influence of the electronic structure of a free radical on complex-formation with a diamagnetic molecule. *Theor. Exp. Chem.* **1978**, *13*, 268–271. [CrossRef]
55. Morishima, I.; Ishihara, K.; Tomishima, K.; Inubushi, T.; Yonezawa, T. Nitroxide radical induced nuclear magnetic resonance contact shift studies. Potential utility of specific downfield ^{1}H contact shifts induced by hydrogen bonding with di-*tert*-butyl nitroxide radical. *J. Am. Chem. Soc.* **1975**, *97*, 2749–2756. [CrossRef]
56. Morishima, I.; Endo, K.; Yonezawa, T. Interaction between closed- and open-shell molecules. VI. ^{1}H and ^{13}C contact shifts and molecular orbital studies on the hydrogen bond of nitroxide radical. *J. Chem. Phys.* **1973**, *58*, 3146–3154. [CrossRef]
57. Knauer, B.R.; Napier, J.J. The nitrogen hyperfine splitting constant of the nitroxide functional group as a solvent polarity parameter. The relative importance for a solvent polarity parameter of its being a cybotactic probe vs. its being a model process. *J. Am. Chem. Soc.* **1976**, *98*, 4395–4400. [CrossRef]
58. Marsh, D. Reaction fields and solvent dependence of the EPR parameters of nitroxides: The microenvironment of spin labels. *J. Magn. Res.* **2008**, *190*, 60–67. [CrossRef]
59. Vogler, A.; Shenderovich, I.G. Photochemistry of deprotonated rhenium(I) (3,3′-dihydroxy-2,2′-bipyridine) tricarbonyl chloride. Photoisomerization at the chelate in basic solution. *Inorg. Chim. Acta* **2014**, *421*, 496–499. [CrossRef]
60. Shenderovich, I.G. Actual Symmetry of Symmetric Molecular Adducts in the Gas Phase, Solution and in the Solid State. *Symmetry* **2021**, *13*, 756. [CrossRef]
61. Gedat, E.; Schreiber, A.; Findenegg, G.H.; Shenderovich, I.; Limbach, H.-H.; Buntkowsky, G. Stray field gradient NMR reveals effects of hydrogen bonding on diffusion coefficients of pyridine in mesoporous silica. *Magn. Res. Chem.* **2001**, *39*, S149–S157. [CrossRef]
62. Shenderovich, I.G.; Denisov, G.S. Modeling of Solute-Solvent Interactions Using an External Electric Field—From Tautomeric Equilibrium in Nonpolar Solvents to the Dissociation of Alkali Metal Halides. *Molecules* **2021**, *26*, 1283. [CrossRef] [PubMed]
63. Morishima, I.; Inubushi, T.; Endo, K.; Yonezawa, T. Interaction between closed and open-shell molecules. V. ^{13}C contact shift and molecular orbital studies on the interaction between halogenated molecules and nitroxide radical. *Chem. Phys. Lett.* **1972**, *14*, 372–376. [CrossRef]
64. Morishima, I.; Inubushi, T.; Endo, K.; Yonezawa, T.; Goto, K. Interaction between Closed- and Open-Shell Molecules. VII. Carbon-13 Contact Shift and Molecular Orbital Studies on the Charge-Transfer Interaction between Halogenated Molecules and Nitroxide Radical. *J. Am. Chem. Soc.* **1972**, *94*, 4812–4818. [CrossRef]
65. Cavallo, G.; Metrangolo, P.; Milani, R.; Pilati, T.; Priimagi, A.; Resnati, G.; Terraneo, G. The Halogen Bond. *Chem. Rev.* **2016**, *116*, 2478–2601. [CrossRef]
66. Grabowski, S.J. Hydrogen and halogen bonds are ruled by the same mechanisms. *Phys. Chem. Chem. Phys.* **2013**, *15*, 7249–7259. [CrossRef]
67. Gleeson, R.; Andersen, C.L.; Rapta, P.; Machata, P.; Christensen, J.B.; Hammerich, O.; Sauer, S.P.A. A Combined Experimental and Theoretical Study of ESR Hyperfine Coupling Constants for N,N,N′,N′-Tetrasubstituted p-Phenylenediamine Radical Cations. *Int. J. Mol. Sci.* **2023**, *24*, 3447. [CrossRef]
68. Khafizov, N.R.; Mukhametgaleev, R.; Madzhidov, T.I.; Kadkin, O.N.; Antipin, I.S. Effect of core substituents on the intramolecular exchange interaction in N,N′-dioxy-2,6-diazaadamantane biradical: DFT studies. *Int. J. Quantum Chem.* **2018**, *118*, e25568. [CrossRef]
69. Shil, S. Effect of deprotonation on the magnetic exchange coupling constant of fluorene-based verdazyl diradical: A computational study. *Int. J. Quantum Chem.* **2018**, *118*, e25543. [CrossRef]
70. Wawer, I.; Kęcki, Z.; Denisow, G.S. Hydrogen bonding in fluoroanilines studied radical probe. *J. Mol. Struct.* **1994**, *327*, 313–319. [CrossRef]
71. Shenderovich, I.G. Electric field effect on ^{31}P NMR magnetic shielding. *J. Chem. Phys.* **2020**, *153*, 184501. [CrossRef]
72. Shenderovich, I.G.; Denisov, G.S. Modeling of the Response of Hydrogen Bond Properties on an External Electric Field: Geometry, NMR Chemical Shift, Spin-Spin Scalar Coupling. *Molecules* **2021**, *26*, 4967. [CrossRef] [PubMed]

73. Shenderovich, I.G.; Denisov, G.S. Adduct under Field—A Qualitative Approach to Account for Solvent Effect on Hydrogen Bonding. *Molecules* **2020**, *25*, 436. [CrossRef] [PubMed]
74. Kolodziejski, W.; Kęcki, Z. ESR and PMR Studies of Alcohols Hydrogen Bonded with Nitroxide Radical. *Ber. Bunsenges. Phys. Chem.* **1978**, *82*, 1312–1314. [CrossRef]
75. Windle, J.J. Hyperfine coupling constants for nitroxide spin probes in water and carbon tetrachloride. *J. Magn. Res.* **1981**, *45*, 432–439. [CrossRef]
76. Malatesta, V.; Ingold, K.U. Protonated nitroxide free radical. *J. Am. Chem. Soc.* **1973**, *95*, 6404–6407. [CrossRef]
77. Uçar, E.; Dadayli, D.; Sünnetçioğlu, M.M.; Sungur, R. An EPR Analysis of Nitroxide Spin Probes in Ethyl Alcohol and Tetrahydrofuran. *Phys. Chem. Liq.* **1999**, *37*, 323–331. [CrossRef]
78. Hoffman, B.M.; Thomas, B.; Eames, T.B. Protonated nitroxide free radical. *J. Am. Chem. Soc.* **1969**, *91*, 2169–2170. [CrossRef]
79. Tachikawa, T.; Akiyama, K.; Yokoyama, C.; Tero-Kubota, S. Local density effects on the hyperfine splitting constant and line width of TEMPO radical in gaseous and supercritical carbon dioxide. *Chem. Phys. Lett.* **2003**, *376*, 350–357. [CrossRef]
80. Sharif, S.; Shenderovich, I.G.; González, L.; Denisov, G.S.; Silverman, D.N.; Limbach, H.-H. NMR and Ab initio Studies of Small Complexes Formed between Water and Pyridine Derivatives in Solid and Liquid Phase. *J. Phys. Chem. A* **2007**, *111*, 6084–6093. [CrossRef]
81. Andreeva, D.V.; Ip, B.; Gurinov, A.A.; Tolstoy, P.M.; Denisov, G.S.; Shenderovich, I.G.; Limbach, H.-H. Geometrical Features of Hydrogen Bonded Complexes Involving Sterically Hindered Pyridines. *J. Phys. Chem. A* **2006**, *110*, 10872–10879. [CrossRef]
82. Ma, Y.; Loyns, C.; Price, P.; Chechik, V. Thermal decay of TEMPO in acidic media via an N-oxoammonium salt intermediate. *Org. Biomol. Chem.* **2011**, *9*, 5573–5578. [CrossRef] [PubMed]
83. Sen', V.D.; Golubev, V.A. Kinetics and mechanism for acid-catalyzed disproportionation of 2,2,6,6-tetramethylpiperidine-1-oxyl. *J. Phys. Org. Chem.* **2009**, *22*, 138–143. [CrossRef]
84. Golubev, V.A.; Rozantsev, É.G.; Neiman, M.B. Some reactions of free iminoxyl radicals with the participation of the unpaired electron. *Russ. Chem. Bull.* **1965**, *14*, 1898–1904. [CrossRef]
85. Hoffman, A.K.; Henderson, A.T. A New Stable Free Radical: DI-t-Butylnitroxide. *J. Am. Chem. Soc.* **1961**, *83*, 4671–4672. [CrossRef]
86. Tupikina, E.Y.; Bodensteiner, M.; Tolstoy, P.M.; Denisov, G.S.; Shenderovich, I.G. P=O Moiety as an Ambidextrous Hydrogen Bond Acceptor. *J. Phys. Chem. C* **2018**, *122*, 1711–1720. [CrossRef]
87. Lyssenko, K.A.; Grintselev-Knyazev, G.V.; Antipin, M.Y. Nature of the P–O Bond in Diphenylphosphonic Acid: Experimental Charge Density and Electron Localization Function Analysis. *Mendeleev Commun.* **2002**, *12*, 128–130. [CrossRef]
88. Chernyshov, I.Y.; Vener, M.V.; Shenderovich, I.G. Local-structure effects on ^{31}P NMR chemical shift tensors in solid state. *J. Chem. Phys.* **2019**, *150*, 144706. [CrossRef]
89. Arp, F.F.; Bhuvanesh, N.; Blümel, J. Hydrogen peroxide adducts of triarylphosphine oxides. *Dalton Trans.* **2019**, *48*, 14312–14325. [CrossRef]
90. Byrne, E.L.; O'Donnell, R.; Gilmore, M.; Artioli, N.; Holbrey, J.D.; Swadźba-Kwaśny, M. Hydrophobic functional liquids based on trioctylphosphine oxide (TOPO) and carboxylic acids. *Phys. Chem. Chem. Phys.* **2020**, *22*, 24744–24763. [CrossRef]
91. Ivshin, K.; Metlushka, K.; Zinnatullin, R.; Nikitina, K.; Pashagin, A.; Zakharychev, D.V.; Efimova, A.; Kiiamov, A.; Latypov, S.; Kataeva, O. Competitive Hydrogen Bonding and Unprecedented Polymorphism in Selected Chiral Phosphorylated Thioureas. *Cryst. Growth Des.* **2021**, *21*, 5460–5471. [CrossRef]
92. Hoefler, J.C.; Vu, A.; Perez, A.J.; Blümel, J. Immobilized di(hydroperoxy)propane adducts of phosphine oxides as traceless and recyclable oxidizing agents. *Appl. Surf. Sci.* **2023**, *629*, 157333. [CrossRef]
93. Borissova, A.O.; Lyssenko, K.A.; Gurinov, A.A.; Shenderovich, I.G. Energy Analysis of Competing Non-Covalent Interaction in 1:1 and 1:2 Adducts of Collidine with Benzoic Acids by Means of X-Ray Diffraction. *Z. Phys. Chem.* **2013**, *227*, 775–790. [CrossRef]
94. Shenderovich, I.G. Weak, Broken, but Working—Intramolecular Hydrogen Bond in 2,2′-bipyridine. *Int. J. Mol. Sci.* **2023**, *24*, 10390. [CrossRef] [PubMed]
95. Lesnichin, S.B.; Tolstoy, P.M.; Limbach, H.-H.; Shenderovich, I.G. Counteranion-Dependent Mechanisms of Intramolecular Proton Transfer in Aprotic Solution. *Phys. Chem. Chem. Phys.* **2010**, *12*, 10373–10379. [CrossRef] [PubMed]
96. Yu, S.; Ward, J.S.; Truong, K.-N.; Rissanen, K. Carbonyl Hypoiodites as Extremely Strong Halogen Bond Donors. *Angew. Chem. Int. Ed.* **2021**, *60*, 20739–20743. [CrossRef]
97. Frisch, M.J.; Trucks, G.W.; Schlegel, H.B.; Scuseria, G.E.; Robb, M.A.; Cheeseman, J.R.; Scalmani, G.; Barone, V.; Petersson, G.A.; Nakatsuji, H.; et al. *Gaussian 09; Revision D.01*; Gaussian, Inc.: Wallingford, CT, USA, 2013.
98. Chai, J.-D.; Head-Gordon, M. Long-range corrected hybrid density functionals with damped atom–atom dispersion corrections. *Phys. Chem. Chem. Phys.* **2008**, *10*, 6615–6620. [CrossRef]
99. Weigend, F.; Ahlrichs, R. Balanced basis sets of split valence, triple zeta valence and quadruple zeta valence quality for H to Rn: Design and assessment of accuracy. *Phys. Chem. Chem. Phys.* **2005**, *7*, 3297–3305. [CrossRef]
100. Dunning, T.H., Jr.; Hay, P.J. Gaussian basis sets for molecular calculations. In *Methods of Electronic Structure Theory*; Schaefer, H.F., Ed.; Springer: New York, NY, USA, 1977; Volume 3, pp. 1–27. [CrossRef]
101. Ernzerhof, M.; Perdew, J.P. Generalized gradient approximation to the angle- and system-averaged exchange hole. *J. Chem. Phys.* **1998**, *109*, 3313–3320. [CrossRef]
102. Shenderovich, I.G. Simplified Calculation Approaches Designed to Reproduce the Geometry of Hydrogen Bonds in Molecular Complexes in Aprotic Solvents. *J. Chem. Phys.* **2018**, *148*, 124313. [CrossRef]

103. Vogler, S.; Dietschreit, J.C.B.; Peters, L.D.M.; Ochsenfeld, C. Important components for accurate pyperfine coupling constants: Electron correlation, dynamic contributions, and solvation effects. *Mol. Phys.* **2020**, *118*, e1772515. [CrossRef]
104. Savitsky, A.; Nalepa, A.; Petrenko, T.; Plato, M.; Möbius, K.; Lubitz, W. Hydrogen-Bonded Complexes of Neutral Nitroxide Radicals with 2-Propanol Studied by Multifrequency EPR/ENDOR. *Appl. Magn. Reason.* **2022**, *53*, 1239–1263. [CrossRef]
105. Möbius, K.; Savitsky, A.; Malferrari, M.; Francia, F.; Mamedov, M.D.; Semenov, A.Y.; Lubitz, W.; Venturoli, G. Soft Dynamic Confinement of Membrane Proteins by Dehydrated Trehalose Matrices: High-Field EPR and Fast-Laser Studies. *Appl. Magn. Reason.* **2020**, *51*, 773–850. [CrossRef]
106. Nalepa, A.; Möbius, K.; Plato, M.; Lubitz, W.; Savitsky, A. Nitroxide Spin Labels—Magnetic Parameters and Hydrogen-Bond Formation: A High-Field EPR and EDNMR Study. *Appl. Magn. Reason.* **2019**, *50*, 1–16. [CrossRef]
107. Wang, K.; He, X.; Rong, C.; Zhong, A.; Liu, S.; Zhao, D. On the origin and nature of internal methyl rotation barriers: An information-theoretic approach study. *Theor. Chem. Acc.* **2022**, *141*, 68. [CrossRef]

Disclaimer/Publisher's Note: The statements, opinions and data contained in all publications are solely those of the individual author(s) and contributor(s) and not of MDPI and/or the editor(s). MDPI and/or the editor(s) disclaim responsibility for any injury to people or property resulting from any ideas, methods, instructions or products referred to in the content.